High-Definition Ion Mobility/Mass Spectrometry with Structural Isotopic Shifts for Nominally Isobaric Isotopologues

Pratima Pathak, Alexandre A. Shvartsburg*

Department of Chemistry and Biochemistry, Wichita State University, 1845 Fairmount, Wichita, KS 67260

* e-mail: alexandre.shvartsburg@wichita.edu

ABSTRACT: We had reported the isotopic envelopes in differential IMS (FAIMS) separations depending on the ion structure. However, this new approach to distinguish isomers was constrained by the unit mass resolution commingling all nominally isobaric isotopologues. Here we directly couple high-definition FAIMS to ultrahigh-resolution (Orbitrap) MS and employ the resulting platform to explore the FAIMS spectra for isotopic fine structure. The peak shifts therein for isotopologues of halogenated anilines with ^{15}N and ^{13}C (split by 6 mDa) in N_2/CO_2 buffers dramatically differ, more than for the ^{13}C, ^{37}Cl, or ^{81}Br species apart by 1 or 2 Da. The shifts in FAIMS space upon different elemental isotopic substitutions are orthogonal mutually and to the underlying separations, forming fingerprint multidimensional matrices and 3-D trajectories across gas compositions that redundantly delineate all isomers considered. The interlocking instrumental and methodological upgrades in this work take the structural isotopic shift approach to the next level.

Introduction

Chemical analyses increasingly focus on the characterization of complex samples in topical areas of proteomics, metabolomics, petroleomics, and environmental monitoring.[1-3] This involves a growing grasp of the ubiquity, diversity, and functional importance of structural isomers.[1-3] Proteins and peptides commonly differ in the position and/or internal structure of post-translational modifications (PTMs) with key biomedical outcomes, eminently for histones where the PTM localization defines the epigenetic function.[4,5] The activities of lipids and smaller biomolecules also vary profoundly across the isomers, e.g., for the trans- versus cis- fats and steroids/hormones relevant to nutrition, health, and sports.[6-8]

Various approaches to characterize the isomeric mixtures have emerged. Most involve multiple stages of mass spectrometry (MS) to delineate the isomers yielding fragment ions with different composition, e.g., for peptides with PTMs on alternative sites.[5,9,10] However, many isomers (e.g., the D/L peptide epimers[11] or lipids with different C=C bond positions or symmetry)[12,13] lead to no distinct fragments. Some others do individually but not in mixtures (e.g., of the three or more peptides with variant PTM localizations, where only those with distal PTMs are identifiable).[10] Such species need to be separated before the MS step. That has been accomplished in the condensed phase by liquid chromatography or electrophoresis,[14] and in gases using ion mobility spectrometry (IMS) that provides unique and often superior selectivity.[7,10,13,15]

The mobility (K) of any ion in a gas depends[16-18] on the electric field strength (E). The IMS techniques can be linear - based on the absolute K at moderate E termed $K(0)$, or differential - resting on the evolution of K at high E levels.[18,19] The differential or field asymmetric waveform IMS (FAIMS) is implemented[17,18] by loading a periodic asymmetric waveform across a gap of width g between two parallel electrodes, with the waveform amplitude (dispersion voltage) U_D producing a peak field of $E_D = U_D/g$. Ions pushed by gas flow are deflected toward either electrode and neutralized on impact. For a given species with certain $K(E)$ form, the drift is offset by fixed compensation field (E_C) due to a dc compensation voltage (U_C) superimposed on the waveform. Thus equilibrated ions pass to a detector (e.g., an MS instrument), while others are still destroyed. Scanning U_C reveals the spectrum of species entering the gap. The resolution maximizes with homogeneous electric field in planar gaps.[18,20] Then the resolving power R_{FAIMS} scales as the square root of filtering time t, controlled by the volume flow rate Q of supplied gas.[20] To compare the data across gap widths, the U_C values are converted to the $E_C = U_C/g$ ratios.

To elucidate the ion structures, one matches the measured K values for resolved species to those calculated for candidate geometries.[21,22] That is enabled by relatively tractable molecular dynamics (MD) in gases as opposed to liquids or on surfaces. As computing small increments of K at high E is much harder than the absolute $K(0)$, the capability has been restricted to linear IMS - mainly in atomic He gas with low polarizability, where a shallow spherical molecular potential simplifies the MD modeling.[21] However, many IMS/MS platforms do not support use of He and procuring it is a growing concern.

Most elements (including H, C, N, O, S which are central to life) have multiple stable isotopes. Their permutations produce numerous isotopologues for nearly all compounds. The ensuing isotopic envelopes were the hallmark of MS since its origins, undergirding various identification and quantification methods.[23,24] The isotopic fine structure apparent in ultrahigh-resolution Fourier-Transform (FT) MS can uniquely identify the molecular formula, but tells nothing about the ion geometry.[25-28] The transposition of isotopic labels over non-equivalent positions creates the isotopomers indistinguishable by MS.

Unlike the motion in vacuum controlled by ion mass (m) and charge, that in gases also depends on the mass distribution. For one, the center-of-mass coordinates in the ion frame affect

all moments of inertia.[29-31] Therefore, the scattering dynamics governing the ion-molecule collision cross sections and thus mobilities differs between the isotopologues/isotopomers in a manner coupled to the ion structure.[29,31] Then one can identify isomers by the splitting of natural isotopic envelopes in FAIMS spectra, quantified via the E_C shifts (ΔE_C) between all observed features (the spreads between E_C values of pertinent isotopologues extracted by MS).[32-36] Same phenomenon was recently noted in linear IMS (specifically cIMS),[37] although with smaller relative inter-isomer differences between the K values - in line with MS generally being more orthogonal to FAIMS than linear IMS.[15] Separations of isotopomers artificially labeled on distinct sites by FAIMS[29,38] and linear IMS (in SLIM[30,31] and cIMS[39] implementations) were also reported.

For the MS-resolved isotopologues, arbitrarily small shifts are fundamentally measurable with any desired precision by collecting replicates.[32-36] Hence, all structural isomers are distinguishable in principle, with the practical limit set by the measurement reproducibility and constraints of sample amount and experimental time.

This paradigm was initially developed utilizing the He/CO_2 buffers and protonated haloanilines with up to three Cl, Br, or I atoms at varied ring positions, producing three or six isomers (m ~ 130 - 330 Da).[32-36] These species display MS features above the base peak by +1 Da (dominated by ^{13}C) and +2 Da (mostly due to ^{37}Cl, ^{81}Br, or $^{13}C_2$ for the iodoanilines with monoisotopic halogen). Some isomers were distinguished by single E_C shifts, and all were delineated by 2-D ($^{13}C/^{37}Cl$ or $^{13}C/^{81}Br$) shifts.[33,35] The shifts for all isotopic groups (save $^{13}C_2$ in few cases)[32-36] were additive, as in:

$$\Delta E_C(^{13}C^{37}Cl) = \Delta E_C(^{13}C) + \Delta E_C(^{37}Cl) \quad (1)$$

This permitted averaging several ΔE_C values in same spectrum, up to $n = 4$ for ^{13}C in tribromoanilines (between m/z of 328 and 329 for sole ^{13}C, 330 and 331 for ^{13}C on top of ^{81}Br, 332 to 333 for ^{13}C on top of $^{81}Br_2$, and 334 to 335 for ^{13}C on top of $^{81}Br_3$).[35] Such multiplexing reduces random ΔE_C errors by ideally the factor of $n^{1/2}$, enhancing the isomer demarcation.[32-36]

Hence, extending the shift matrices to new isotopes and extra instances of the same isotopes helps. One avenue is improving the sensitivity and useful range of ion intensities (dynamic range, dr) to cover more rare isotopologues. For example,[33] the protonated dichloroanilines $C_6H_6NCl_2^+$ (DCAs) feature within dr ~ 100 six isotopic peaks at unit (integer) masses: m/z = 162, 163 (mainly due to ^{13}C), 164 (^{37}Cl), 165 ($^{13}C^{37}Cl$), 166 ($^{37}Cl_2$), 167 ($^{13}C^{37}Cl_2$). The dr = 5,000 achieved in the high-definition FAIMS/MS platform brings in the peak at m/z = 168 (primarily due to $^{13}C_2{}^{37}Cl_2$). However, the E_C values for weaker peaks are less certain, and incorporating them into the statistics often worsens the E_C error margin.

Many isotopologues are nominally isobaric: e.g., the D, ^{13}C, ^{15}N, or ^{17}O substitutions add 1 Da, while $^{13}C_2$, ^{18}O, ^{37}Cl, or ^{81}Br add 2 Da. Thus the number of isotopologues exceeds that of unit-mass peaks with the same minimal abundance. For instance,[33] there are 15 exact-mass DCA peaks within dr = 5,000. The eight new species replace ^{13}C by ^{15}N (at m/z = 163, 165, 167 with the mass difference Δm = –6 mDa), ^{13}C by D (at m/z = 163 and 165 with Δm = 3 mDa), ^{37}Cl by $^{13}C_2$ (at m/z = 164 and 166 with Δm = 9 mDa), or ^{37}Cl by $^{13}C^{15}N$ (at m/z = 164 with Δm = 3 mDa). With $|\Delta m| \le 9$ mDa, these isotopologues fully merge in ion trap MS even in the ultrazoom mode (R_{MS} ~ 1000).[32-36] Besides the loss of information about their E_C shifts, such contamination affects the ΔE_C values ascribed to the major isotopologues at unit masses. The deviation must be minor for haloanilines with single isotopologues contributing >90% of signal at each unit mass,[32-36] but not species with comparably abundant nominal isobars. For example, the peak at m/z = 167 for deprotonated phthalic acids ($C_8H_5O_4^-$, base m/z = 165) comprises the isotopologues with ^{18}O and $^{13}C_2$ in 70:29 ratio.

The mass splits of ≥3 mDa for DCAs[33] could be resolved with R_{MS} > 100,000 routinely available from FTMS (including Orbitrap MS) instruments. Some isotopologues in other formulas lie closer, e.g., those with ^{37}Cl versus ^{81}Br differ by 0.9 mDa. Disentangling such species hinges on higher R_{MS} reachable by FTMS. The systems with $R_{MS} \sim 10^6$ reveal complete isotopic distributions for essentially all species in the mass range up to ~500 Da where the E_C shifts in FAIMS have been encountered.[27,28,35] Hence, the construction of comprehensive ΔE_C matrices using FAIMS/FTMS platforms is paramount to the progress of the structural isotopic shift approach.

We preferred the He/N_2 buffers for conventional FAIMS separations and He/CO_2 for isotopic analyses.[32-36] Such buffers containing light and heavy gases tend to augment the resolution because of non-Blanc effects (deviations from the Blanc's law of diffusion at high electric fields, prominent in mixtures of disparate gases),[40] but are incompatible with ultrahigh vacuum pumping of Orbitrap MS. Hence, combining high-definition FAIMS with Orbitrap MS necessitated the pumping modifications and/or a tandem electrodynamic ion funnel interface (IFI) to dilute He with heavier gases.[10] A substantial He consumption involved is also problematic with growing helium shortage.

The high-resolution FAIMS/FTMS capability has been exploited in proteomics.[10] Here, we augment the MS resolution further and expand to the isotopic analyses, leveraging the ultrahigh MS resolution to disentangle the FAIMS peaks for nominal isobars. A modern Orbitrap model with rf-focusing front interface allows attaching the FAIMS stage directly, while the N_2/CO_2 buffers also deliver structurally specific isotopic shifts.

Experimental Methods

A planar FAIMS stage (g = 1.88 mm) runs at the atmospheric pressure and lab temperature (~20 °C).[41] We previously joined it to the XL ion trap or Orbitrap MS instruments.[10,29,32-36,38,41] Replacing their skimmer/orifice inlet by IFI has raised the ion transmission, but complicated the assembly and operation of high-resolution FAIMS/MS platforms. Here we employ the LTQ Velos/Orbitrap Elite MS instrument with the S-lens front end that (although inferior to an IFI) suffices in the targeted m/z range.[42] We have thus removed the electrospray ionization (ESI) source and mounted on its holding rods a PEEK bracket securing the FAIMS stage to face the MS inlet capillary with a 2.5 mm spacing (Figure S1). This design allows switching between the FAIMS/MS and MS regimes in seconds without breaking vacuum.

The FAIMS cell was biased at 30 V (above the grounded MS inlet) with the curtain plate at 1 kV. Ions came from a syringe-driven ESI emitter placed in front of the aperture in that plate and set at 5 kV.[32-36,41] A bisinusoidal waveform (1 MHz frequency, 2:1 harmonics ratio) had U_D of 5.5 kV. The U_C windows with ion signal were scanned at the rate Sr of 1 V/min.

The N_2/CO_2 mixtures were formulated by digital flowmeters (MKS Instruments) and purified by a GC filter (Agilent, RMSN-4). Since He has a minimal arc breakdown threshold (<1

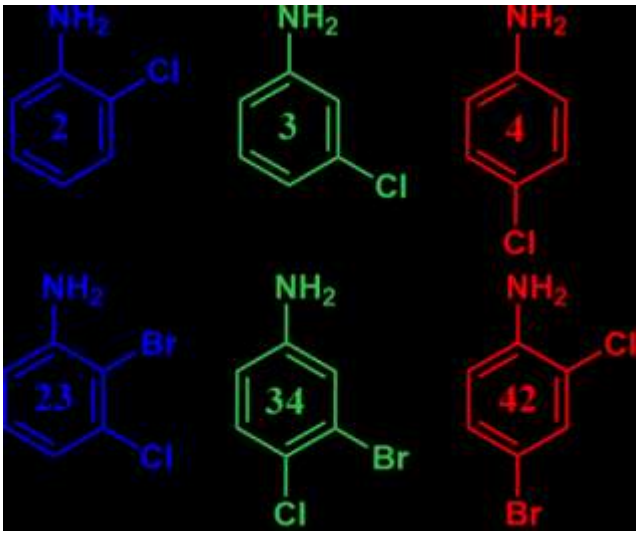

Figure 1. The MCA and BCA isomers treated in this work.

kV for the present gap), the He fraction used in FAIMS must be limited - commonly to 50 - 70% in media with N_2 or CO_2. The much greater thresholds for N_2 and CO_2 (~7 kV here)[43] permit analyses over the full composition range.

Ions can be suitably desolvated in the curtain plate inlet and injected into this FAIMS cell at $Q \sim 0.5$ - 4 L/min, for $t \sim 70$ - 600 ms.[44] Here we adopt $Q = 3$ L/min near the top of said range. The associated $t \sim 100$ ms is below our normal ~150 ms at $Q =$ 2 L/min, elevating the ion signal and *dr* to capture the minor isotopologues.[36,44] A concomitant slightly reduced resolution is acceptable in isotopic shift analyses with the juxtaposed peaks distinguished by MS.

To connect to prior studies, we probe the protonated monochloroanilines $C_6H_7NCl^+$ (MCAs) investigated earlier and similar bromochloroanilines $C_6H_6NBrCl^+$ (BCAs) with monoisotopic masses of 128 and 206 Da. We look at all MCA isomers (ortho **2**, para **3**, meta **4**) and three of the ten BCAs (2-bromo-3-chloro **23**, 3-bromo-4-chloro **34**, 4-bromo-2-chloro **42**) purchased from Sigma or TCI, Figure 1. The 100 µM solutions of standards or mixtures in methanol with 1% formic acid were infused to the emitter at 0.5 uL/min. This high concentration maximizes the ion counts for sufficient statistics even for the isotopic traces. The E_C axis was anchored by linear dilation using the 2-monobromoaniline (MBA) calibrant spiked at 50 µM.

The precision of extracted E_C shifts is determined by that of corresponding peak positions. We typically set those as the midpoints at half maximum. More detailed descriptions combining the midpoints at multiple heights (e.g., 25% and 50%) reduce the random error due to ion flux fluctuations.[36] The ultimate (albeit laborious) method of numerical peak integration was not employed in the preceding analyses. These sophisticated formalisms are more important for weaker features with less stable signal. Here we integrate the smallest features with the ^{15}N atoms but adopt the midpoints at half-height for other peaks.

To improve the accuracy of measured E_C shifts and assess their statistics (the 95% confidence intervals throughout the paper), we collected 10 - 30 spectral replicates.[32-36]

Table 1. Relative intensities (*I*) computed for H^+MCA and H^+BCA isotopologues (using the utility on www.sisweb.com).

Heavy Atoms	Exact mass		Unit mass		% at# unit *m*
	m, Da	*I**	*m*, Da	*I**	
MCAs					
None	128.027	**100**	128	100	100
^{15}N	129.024	**0.361**	129	6.96	**5.18**
^{13}C	129.030	**6.489**			**93.19**
D	129.033	**0.112**			1.61
^{37}Cl	130.024	**32.40**	130	32.6	99.37
$^{13}C^{15}N$	130.027	**0.023**			0.07
$^{13}C_2$	130.033	**0.175**			0.54
^{13}CD	130.036	0.007			0.02
$^{37}Cl^{15}N$	131.021	**0.117**	131	2.26	**5.18**
$^{37}Cl^{13}C$	131.027	**2.102**			**93.05**
^{37}ClD	131.030	**0.036**			1.61
$^{13}C_3$	131.037	0.0025			0.11
$^{37}Cl^{13}C^{15}N$	132.024	0.0076	132	0.07	11
$^{37}Cl^{13}C_2$	132.030	**0.057**			85
$^{37}Cl^{13}CD$	132.033	0.0024			4
BCAs					
None	205.937	**100**	206	100	100
^{15}N	206.934	**0.361**	207	6.95	**5.20**
^{13}C	206.941	**6.489**			**93.42**
D	206.943	**0.096**			1.38
^{37}Cl	207.934	**32.40**	208	130	24.90
^{81}Br	207.935	**97.51**			74.94
$^{13}C^{15}N$	207.938	**0.023**			0.02
$^{13}C_2$	207.944	**0.175**			0.13
^{13}CD	207.947	0.006			0.005
$^{37}Cl^{15}N$	208.931	**0.117**	209	9.03	**1.30**
$^{81}Br^{15}N$	208.932	**0.352**			**3.90**
$^{37}Cl^{13}C$	208.938	**2.102**			**23.29**
$^{81}Br^{13}C$	208.939	**6.328**			**70.10**
^{37}ClD	208.941	**0.031**			0.34
^{81}BrD	208.941	**0.094**			1.04
$^{13}C_3$	208.947	0.003			0.03
$^{37}Cl^{81}Br$	209.932	**31.59**	210	31.9	99.15
$^{37}Cl^{13}C^{15}N$	209.936	0.008			0.03
$^{81}Br^{13}C^{15}N$	209.936	**0.023**			0.07
$^{37}Cl^{13}C_2$	209.941	**0.057**			0.18
$^{81}Br^{13}C_2$	209.942	**0.171**			0.54
$^{81}Br^{13}CD$	209.945	0.006			0.02
$^{37}Cl^{81}Br^{15}N$	210.929	**0.114**	211	2.19	**5.20**
$^{37}Cl^{81}Br^{13}C$	210.936	**2.05**			**93.44**
$^{37}Cl^{81}BrD$	210.938	**0.03**			1.37
$^{37}Cl^{81}Br$ $^{13}C^{15}N$	211.933	0.007	212	0.06	11
$^{37}Cl^{81}Br^{13}C_2$	211.939	**0.055**			89

* Intensity relative to the base peak (100%) for all species with $I^* \geq 0.002\%$. The I^* values $\geq 0.02\%$ are bolded. # The nominal isobars comprising ^{15}N versus ^{13}C presently resolved by MS are in green and blue fonts, respectively.

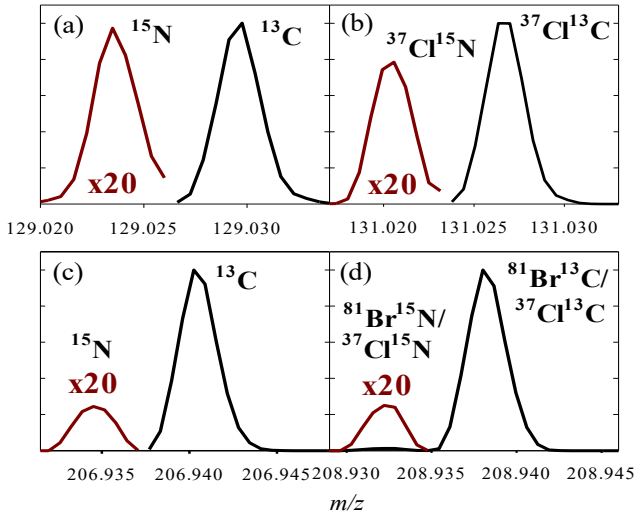

Figure 2. Normalized MS spectral windows for MCA (a, b) and BCA (c, d) showing the isotopologues with one ^{13}C (black) or ^{15}N (brown, expanded scale) atom. Full spectra are in Figure S3.

Results and Discussion

Isotopic envelopes and mass spectra

The *a priori* isotopic distributions for MCA and BCA ions show a fine structure with multiple significant isotopologues at all unit masses above the base peak (Table 1). Within dr = 5,000, transitioning from unit to exact masses lifts the number of compositions from 5 to 11 (for MCAs), 5 to 12 (MBAs), 7 to 15 (DCAs), 7 to 22 (BCAs), 7 to 16 (dibromoanilines, DBAs), and 9 to 22 (TBAs).[32-36] Expanding the number of isotopologues by 2 - 3× portends well for the isotopic shift analyses.

The nominal R_{MS} of Elite (at m/z = 400) is up to 240,000. With the $R_{MS} \propto (m/z)^{-1/2}$ scaling in Orbitraps, the theoretical R_{MS} and full peak width at half maximum (w) are ~420,000 and 0.3 mDa for MCAs and ~330,000 and 0.6 mDa for BCAs. These w values match the observations (Figure S2). Assuming a criterion of $\Delta m \geq 2w$, this would allow resolving all isotopologues in Table 1 except the BCAs with ^{37}Cl vs. ^{81}Br (Δm = 0.9 mDa) which indeed merged (Figure S2). The species with ^{15}N and ^{13}C (Δm = 6 mDa), including those comprising the ^{37}Cl and/or ^{81}Br atoms, were resolved. Others were not detected with enough signal, presumably because of low abundance and/or coalescence[45] that commonly reduces the resolution of close peaks in FTMS below that inferred from the single-peak widths. Thus the number of actually discerned isotopologues was smaller: 7 for MCAs and 10 for BCAs.

The species with ^{15}N and ^{13}C remained resolved baseline at set R_{MS} = 60 K for both MCAs (with w = 1.2 mDa) and BCAs (w = 2.4 mDa), but with greater signal given the resolution/sensitivity trade-off in Orbitrap MS. Otherwise, the mass spectra (Figures 2, S3) followed the Table 1 and low-resolution data for MCAs.[32] We selected this condition for FAIMS analyses.

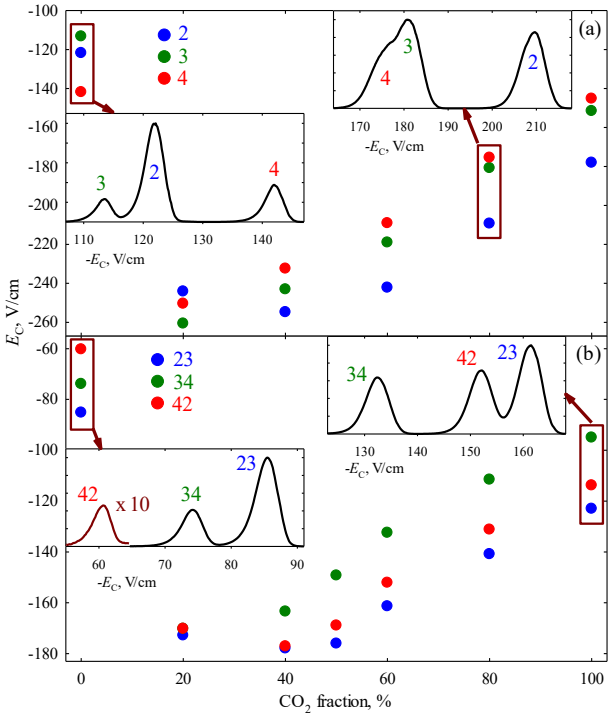

Figure 3. Measured E_C values for MCA (a) and BCA (b) isomers over the full N_2/CO_2 composition range. The FAIMS spectra at selected CO_2 fractions are in insets.

FAIMS separations

Ions up to ~200 Da normally behave[46,47] as type A (where K increases at higher E yielding $E_C < 0$) in both N_2 and CO_2, with greater absolute E_C values in more polarizable CO_2 as deeper ion-molecule potentials augment the difference between low- and high- energy scattering patterns.[46] This applies to all MCAs and BCAs here (Figure 3). The values in N_2/CO_2 mixtures substantially exceed those in either gas because of the non-Blanc effect in high-field ion mobility, maximizing at the compositions with smaller fraction of heavier gas (here ~20 - 40% CO_2).[40] The peak order for MCA or BCA isomers changes between N_2 and CO_2, specifically near 20% CO_2. These trends track those for the three phthalic acid isomer anions with varying position of a substituent (there carboxyl) on the benzene ring.[48] The maximum $|E_C|$ for MCAs (~260 V/cm) lies below ~300 V/cm reached in He/CO_2 buffers with a more pronounced non-Blanc effect because of greater physical disparity between the components and their interaction potentials with ions,[40] but the order of $|E_C|$ values at ≥40% CO_2 here (**2** > **3** > **4**) copies that in He/CO_2 mixtures. The maximum for BCAs (~180 V/cm) is lower as anticipated for heavier type A species.[46] With w scaling approximately as $K^{-1/2}$ in planar FAIMS analyzers[20] and ion mobilities lower in CO_2 than N_2 with smaller mass and cross section, adding CO_2 broadens the peaks. All isomers were separated baseline in N_2 or at 40 - 60% CO_2. The resolution near 20% CO_2 is hampered by peak transposition, whereas at the highest fractions the peak capacity is diminished by dropping E_C values and wider peaks.

Isotopic shifts for MCAs

Both ^{13}C and ^{37}Cl shifts in all N_2/CO_2 compositions are positive (Figure 4) as in He/CO_2 buffers.[32,34] The ^{13}C shifts rise from the minimal 0.1 - 0.4 V/cm in N_2 to 1.1 - 2.0 V/cm at 40 -

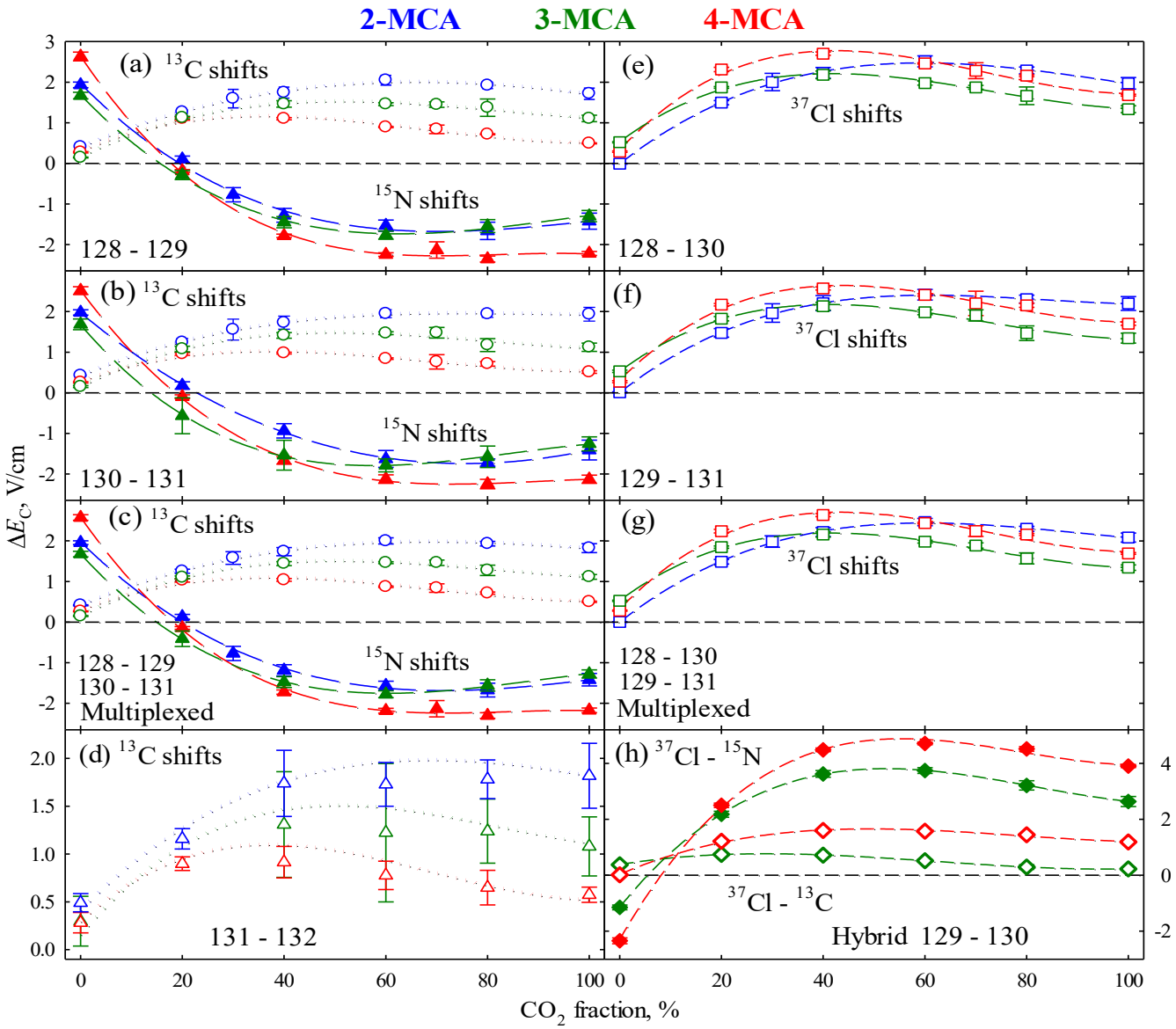

Figure 4. Measured E_C shifts in the MCAs for ^{13}C (circles, a - d), ^{15}N (triangles, a - d), ^{37}Cl (squares, e - g), ^{37}Cl – ^{13}C (empty diamonds, h), and ^{37}Cl – ^{15}N (filled diamonds, h). Error bars show the 95% confidence intervals. Black lines mark $\Delta E_C = 0$. Colored lines are cubic regressions through the data. The shifts with "from - to" m/z values are labeled.

60% CO_2 and slide down to 0.5 - 1.7 V/cm in CO_2 (a, b). The ranking of ΔE_C at ≥40% CO_2 is **2** > **3** > **4**, same as in He/CO_2 buffers and matching the order of $|E_C|$ values. This ranking stays at 20% CO_2, where it differs from that of $|E_C|$ values (**3** > **4** > **2**), and changes in N_2 to **2** > **4** > **3** that still differs from the flipped $|E_C|$ order (**4** > **2** > **3**). The ^{13}C shifts in the isotopologues with ^{35}Cl (from m/z of 128 to 129, Figure 4a) and ^{37}Cl (from m/z of 130 to 131, Figure 4b) are virtually identical, as found for all species in He/CO_2 buffers.[32,34] This again permits multiplexing the shifts to compress the error margins and thus improve specificity (Figure 4c): the mean 95% confidence intervals narrow by 1.3× which is close to the $2^{1/2}$ = 1.4 (Table S1). The actual multiplexing gain from the baseline for shift between two most intense peaks would be under the $n^{1/2}$ factor[49] because the added shifts between less intense peaks (here, at m/z = 130 and 131) have greater statistical uncertainties (Table S1).

The shifts for the second ^{13}C atom (measurable between m/z of 131 and 132 in the isotopologues with ^{37}Cl, Figure 4d) are close, but much wider E_C uncertainties due to low signal (<0.1% of the base peak) make averaging them in counterproductive (Table S1).

The ^{37}Cl shifts increase from 0.0 - 0.5 V/cm in N_2 to maxima of 2.2 - 2.7 V/cm at 40 - 60% CO_2, then decrease to 1.3 - 2.0 V/cm in CO_2 (Figure 4e). This resembles the trend for ^{13}C shifts, but with moderately higher magnitudes across the gas compositions – also per the pattern with He/CO_2 buffers.[32,34] The ΔE_C ranking evolves from **3** > **4** > **2** in N_2 to **4** > **3** > **2** around 20% CO_2 to **4** > **2** > **3** near 50% CO_2 and finally **2** > **4** > **3** at >60% CO_2. The ranks in N_2 or CO_2 differ from those for ^{13}C shifts and the $|E_C|$ orders: distinct elemental shifts are orthogonal mutually and to the underlying separations. Heretofore, we combined the ΔE_C for ^{13}C on top of the ^{37}Cl or ^{81}Br atom(s), but not vice versa. Here, the ^{37}Cl shifts in species with ^{13}C (from m/z of 129 to 131, Figure 4f) follow those in species with ^{12}C (from m/z of 128 to 130). The ensuing multiplexing expectedly reduces the uncertainties (Figure 4g), also by 1.3× (Table S1). This clarifies the previously ambiguous[32,34] rank of shifts for **3** and **4** in CO_2.

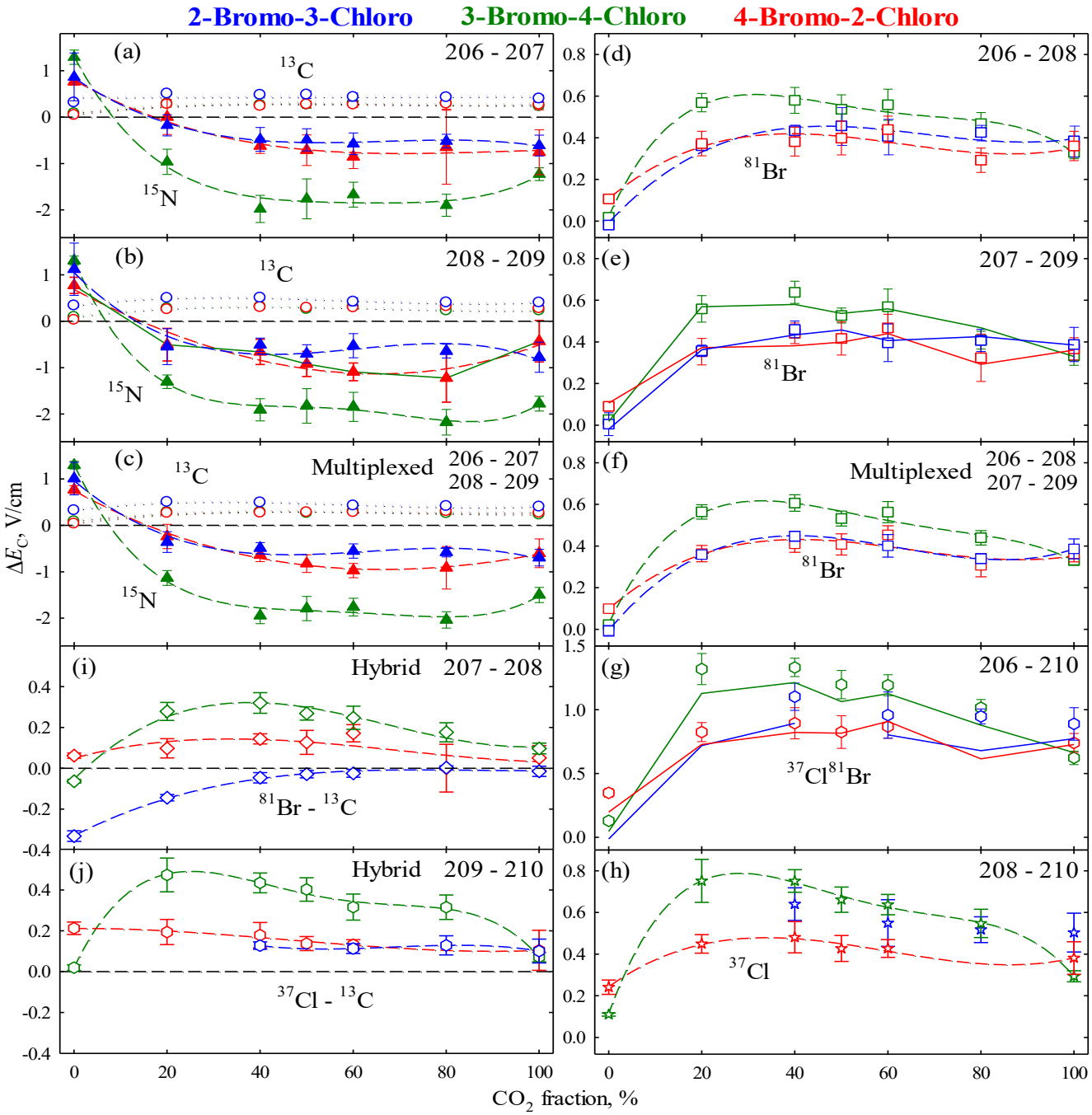

Figure 5. Same as Figure 4 for BCAs, with the shifts for ^{13}C (circles, a - c), ^{15}N (triangles, a - c), ^{81}Br (squares, d - f), ^{37}Cl^{81}Br (hexagons, g), ^{37}Cl (stars, h), ^{81}Br – ^{13}C (diamonds, i), ^{37}Cl – ^{13}C (hexagons, j). Solid lines in (e) and (g) transfer the symbols from (d) and (f), respectively.

The MS resolution of nominal isobars now enables isolating the ^{15}N shifts (Figure 4 a, b). These are highly positive (1.7 - 2.6 V/cm) in N_2 but rapidly drop upon CO_2 addition, crossing into the negative range at ~20% CO_2 and reaching –(1.7 - 2.4) V/cm at 60% CO_2, then stay flat or move slightly toward zero up to pure CO_2. The uncertainties significantly exceed those of ^{13}C or ^{37}Cl shifts because of low signal (Table S1). Nonetheless, the ΔE_C rank can be established: **4** > **2** > **3** in N_2, **2** > **3** > **4** at 40 - 60% CO_2, and **3** ≥ **2** > **4** at ≥80% CO_2. Once more, the shifts for ^{15}N on top of ^{35}Cl (Figure 4a) and ^{37}Cl (Figure 4b) are similar, and their multiplexing compresses the error margin (Figure 4c, Table S1).

When the E_C shifts upon different isotopic substitutions have inter-isomer spreads of opposite signs, the shift between the resulting two peaks can be greater and more specific than those upon either heavy-atom substitution. This applies to the {^{13}C; ^{37}Cl} and {^{15}N; ^{37}Cl} pairs for **3** and **4** in most gas compositions, and the hybrid shifts (from the proper peak at *m/z* of 129 to 130) are indeed more informative (Figure 4h). For example, the (^{37}Cl – ^{15}N) shifts are larger than ^{15}N shifts but have smaller uncertainties (Table S1). The {^{13}C; ^{15}N} pair is not useful here because of same ^{13}C and ^{15}N shift rankings at most CO_2 fractions.

The best isomer assignments come from the multiplexed ^{13}C shifts at ≥60% CO_2 (Figure 4c), with **3** and **4** redundantly delineated by the (^{37}Cl – ^{13}C) and (^{37}Cl – ^{15}N) hybrid shifts. Hence, the ^{15}N shifts aid but are not critical to the MCA isomer identification. The utility of a certain shift may vary across the isomer groups even within similar compounds: e.g., the ^{37}Cl shifts are more specific for di- than mono- haloanilines.[33] Same holds for the ^{15}N shifts in BCAs.

Isotopic shifts for BCAs

The ^{13}C shifts for BCAs also stay positive in all gas compositions, rising from 0 to ~40% CO_2 and then flattening or slightly diminishing up to pure CO_2 (Figure 5 a - c). Their magnitudes (0.0 - 0.3 V/cm in N_2, 0.3 - 0.5 V/cm at maximum, 0.2 – 0.4 V/cm in CO_2) are below the values for MCAs, expectedly for heavier ions.[34-36] The consistent rank **23** > **34** ≅ **42** enables the demarcation of **23** from the other two, but not therebetween. The ΔE_C for ^{13}C on top of $^{35}Cl^{79}Br$ (Figure 5a) and $^{35}Cl^{81}Br/^{37}Cl^{79}Br$ (Figure 5b) are again similar, and multiplexing reduces the uncertainty (Figure 5c, Table S2).

With the species comprising ^{37}Cl versus ^{81}Br unresolved by MS, we ascribe the shifts for their joint peak to ^{81}Br as the major constituent (Table 1). Those overall resemble the ^{13}C shifts, inching up from 0.0 - 0.1 V/cm in N_2 to the maxima of 0.4 - 0.6 V/cm near 40% CO_2 and decreasing to 0.4 V/cm in CO_2 (Figure 5 d - f). This pattern of somewhat greater shifts for the heavy halogen than ^{13}C copies that in MCAs or MBAs.[32,34] The ^{81}Br shift for **34** exceeds the (close) values for **23** and **42** at 20 - 80% CO_2, but is higher for **42** than **23** or **34** in N_2. The shifts for ^{81}Br on top of ^{13}C (Figure 5e) confirm those on top of ^{12}C (Figure 5d) and allow multiplexing for improved definition (Figure 5f, Table S2).

The ΔE_C values for $^{37}Cl^{81}Br$ (from m/z of 206 to 210, Figure 5g) for all isomers lie slightly above $2\Delta E_C$ for ^{81}Br. Hence, the ^{37}Cl shifts, which can be obtained by subtraction, track but exceed the ^{81}Br shifts (Figure 5h). The same was seen for MCAs versus MBAs[34] and DCAs vs. DBAs,[35] likely reflecting a larger relative value of 2 Da mass increment (5.7% for ^{35}Cl vs. 2.5% for ^{79}Br). The ^{37}Cl shifts resolve **34** vs. **42** at 20 - 80% CO_2 better than the ^{81}Br shifts, but cannot resolve **23** from **34**.

Once more, the inter-isomer distinctions can be magnified in judiciously picked hybrid shifts. Our three BCAs are reasonably delineated by the (^{81}Br – ^{13}C) shifts in N_2 and at 20 - 50% CO_2, including the **34** and **42** swapping order between N_2 and 20% CO_2 (Figure 5i). The (^{37}Cl – ^{13}C) shifts improve the resolution of **34** vs **42**, but again do not resolve **23** from **34** (Figure 5j). Unlike with MCAs, no combination of ^{13}C and heavy halogen shifts reliably distinguishes all three isomers in CO_2.

Now the ^{15}N shifts elicited with FTMS become crucial. These have $\Delta E_C > 0$ in N_2, but rapidly drop into the negative territory up to ~50% CO_2 and then stay near-flat to 100% CO_2 (Figure 5 a - c). The shifts for ^{15}N on top of ^{79}Br (Figure 5a) and ^{81}Br (Figure 5b) match, allowing multiplexing (Figure 5c, Table S2). All this reprises the picture for MCAs with expectedly smaller absolute ΔE_C for heavier ions: 0.8 - 1.3 V/cm at the maxima and –(0.7 - 2) V/cm at the minima. However, the shifts are more specific for these BCAs than MCAs: that for **34** lies well below those for **23** and **42** at ≥20% CO_2 to easily differentiate **34** up to 100% CO_2. With that, all three BCA isomers are distinguishable in any N_2/CO_2 composition.

Conclusions

We coupled high-definition FAIMS to MS (and particularly Orbitrap MS) instruments with the S-lens inlet as is, facilitating FAIMS/MS analyses with high 2-D resolution. This platform was deployed to disentangle the FAIMS spectra for nominally isobaric isotopologues resolved by FTMS, building on the isomer characterization by the shifts for species at unit masses.[32-36] We also took this concept beyond the initial He/CO_2 buffers to the readily available and inexpensive N_2/CO_2 mixtures.

Six monochloroaniline (MCA) and bromochloroaniline (BCA) isomers were separated baseline, with the resolution dampened at greater CO_2 fractions. All isotopologues with ^{13}C, ^{15}N, ^{37}Cl, and/or ^{81}Br exhibit material shifts in mass-selected FAIMS spectra, with ^{13}C and ^{15}N (Δm = 6 mDa) fully resolved by Orbitrap MS. The absolute shifts tend to increase from N_2 to CO_2 to N_2/CO_2 mixtures, in concord with generic projections of stronger isotopic effects in heavier gases[50] and steeper nonlinearity of mobility in gas mixtures expanding the separation space.[40] As with He/CO_2 buffers,[32-36] the elemental shifts are additive and can be multiplexed for best isomer demarcation. This evidently universal property of FAIMS may prove key to rationalizing and predicting the isotopic shifts. These shifts are orthogonal to the underlying separations and each other, making up matrices of exceptional structural specificity.

All MCAs and BCAs can be distinguished by the $^{13}C/^{37}Cl$ or $^{13}C/^{81}Br$ shifts over a range of N_2/CO_2 compositions. The hybrid shifts reflecting multiple isotopic substitutions (such as ^{37}Cl – ^{13}C) are even more specific for certain isomers. The gas composition dimension, with the shifts switching order or sign at certain points, enhances the specificity further.

The novel ^{15}N shifts isolated by Orbitrap MS are almost opposite to the ^{13}C shifts at >20% CO_2 fractions. This observation defies simple rationalization. As the N atom lies outside the C ring, the ^{15}N substitution moves the ion center-of-mass (COM) more than the ^{13}C substitution averaged over carbons. However, the Cl or Br atoms are in similar positions to N and (with +2 Da mass increments) the ^{37}Cl and ^{81}Br substitutions cause even greater COM transpositions, yet the ^{37}Cl, ^{81}Br, and ^{13}C shifts are positive and overall similar. As the ^{15}N shift becomes strongly positive in N_2, the ion-molecule collision dynamics beyond the COM transposition is critical.

This means mutual shifts well above those between the ^{13}C and ^{37}Cl or ^{81}Br peaks differing by 1 Da, showcasing the independence of isotopic shifts in FAIMS of the mass difference. The ^{15}N shifts pull apart the BCA isomers in CO_2 (where other shifts fall short) and furnish redundant confirmation across the board.

The two isotopic shifts across binary gas compositions are succinctly conveyed as paths on a map.[35] The three shifts, including the ^{15}N revealed here using FTMS, can be represented by the 3-D trajectories (Figure 6). The MCA and BCA isomers are trivially distinguished in these spatial plots. Their projections on the coordinate planes yield three 2-D maps (Figures S4, S5). Their distinct patterns reemphasize the benefit from additional shifts and namely ^{15}N, e.g., the paths for **3** and **4** intersect in the $^{13}C/^{35}Cl$ and $^{13}C/^{15}N$, but not $^{35}Cl/^{15}N$ maps (Figure S4).

Separations of isotopomers by linear IMS are correlated to the COM movement within the ion.[31] Same was hypothesized to underpin the isotopic shifts in FAIMS,[29,32] but the ordering of isomers by shift in linear IMS and FAIMS differed: e.g., that for ^{37}Cl shift in DCAs was 2,5 < 2,4 < 3,4 < 3,5 in linear IMS[37]

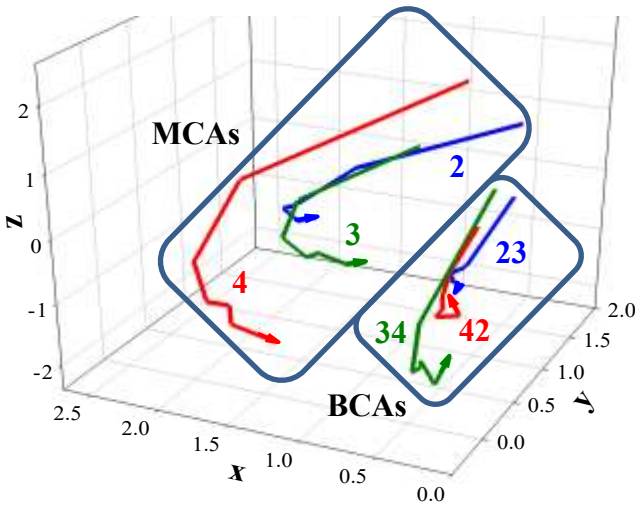

Figure 6. The 3-D plot of isotopic shifts (^{13}C - **y**, ^{37}Cl/^{81}Br - **x**, ^{15}N - **z**) in V/cm for MCAs and BCAs in N_2/CO_2 buffers (directions to CO_2 marked).

but 2,4 = 3,4 < 3,5 ≅ 2,5 in FAIMS.[33] However, those studies employed N_2 buffer for linear IMS but He/CO_2 for FAIMS, and present data show the reordering of shift magnitudes (including for ^{37}Cl) between the N_2 and CO_2 gases. Hence, to what extent the distinct orders above manifested the inherent orthogonality of FAIMS to linear IMS[37] versus that of shifts across gases remains to be deduced. Again, the isotopic shift models ought to examine the ion-molecule collision dynamics beyond the COM transpositions.

The IMS isotopic shift approach is physically unrelated but operationally analogous to NMR, where multiple chemical shifts carry complementary information about the molecular structure.[32-34] Then the current advance could be likened to opening NMR to many active nuclei beyond ^{13}C, including ^{15}N. The advantages and challenges of ^{15}N shifts here mirror those for ^{15}N-NMR: superior selectivity and inferior sensitivity stemming from low abundance of ^{15}N versus ^{13}C due to fewer N sites and smaller heavy isotope population (0.3% vs 1.0%).[51] Nonetheless, the NMR methods relying on ^{15}N shifts (alone and correlated with others including ^{13}C) have proliferated.[52] Some studies improve the sensitivity using the ^{15}N labeling.[52] That can likewise apply to the FAIMS isotopic shifts.

We are taking the isotopic shift analyses to regular non-halogenated organic compounds, including the carboxylic acids and other oxygenated species (with ^{17}O and ^{18}O stable isotopes). Future work will use superior FTMS platforms (R_{MS} ≥ 500,000) to elicit the shifts for isotopologues closer in mass, e.g., comprising ^{13}C versus D (Δm = 2.9 mDa) or ^{17}O (Δm = 0.8 mDa), or $^{13}C_2$ versus ^{18}O (Δm = 2.4 mDa). Such new shifts will expand the 3-D plots into hypercubes. The isotopic fine structure may become as important to IMS as it is to MS, especially for heavier ions with more isotopologues per unit mass.

ACKNOWLEDGMENT

This research was funded by NSF (CHE-2105182). We thank Gordon A. Anderson (GAACE) and Hayden Thurman and Walin Moorsol (WSU) for experimental help, and Alexander Makarov (Thermo) and Yuri Tsybin (Spectroswiss) for insightful discussions on the isotopic resolution by Orbitrap MS.

Supporting Information

Additional mass spectra, table of ΔE_C uncertainties, 2-D shift maps.

REFERENCES

1. Seydel, C. Diving Deeper into the Proteome. *Nat. Methods* **2022**, *19*, 1036.
2. Heiles, S. Advanced Tandem Mass Spectrometry in Metabolomics and Lipidomics - Methods and Applications. *Anal. Bioanal. Chem.* **2021**, *413*, 5927.
3. Marshall, A. G.; Rodgers, R. P. Petroleomics: Chemistry of the Underworld. *Proc. Nat. Acad. Sci. USA* **2008**, *105*, 18090.
4. Jenuwein, T.; Allis, C. E. Translating the Histone Code. *Science* **2001**, *293*, 1074.
5. Olsen, J. V.; Mann, M. Status of Large-Scale Analysis of Post-Translational Modifications by Mass Spectrometry. *Mol. Cell. Proteomics* **2013**, *12*, 3444.
6. Oteng, A. B.; Kersten, S. Mechanisms of Action of *trans* Fatty Acids. *Adv. Nutr.* **2020**, *11*, 697.
7. Harris, R. A.; Leaptrot, K. L.; May, J. C.; McLean, J. A. New Frontiers in Lipidomics Analyses Using Structurally Selective Ion Mobility - Mass Spectrometry. *Trends Analyt. Chem.* **2019**, *116*, 316.
8. Ray, J. A., Kushnir, M. M., Yost, R. A., Rockwood, A. L., Meikle, A. W. Performance enhancement in the measurement of 5 endogenous steroids by LC-MS/MS combined with differential ion mobility spectrometry. *Clin. Chim. Acta* **2015**, *438*, 330.
9. Taverna, S. D.; Ueberheide, B. M.; Liu, Y.; Tackett, A. J.; Diaz, R. L.; Shabanowitz, J.; Chait, B. T.; Hunt, D. F.; Allis, C. D. Long-Distance Combinatorial Linkage between Methylation and Acetylation on Histone H3 N Termini. *Proc. Nat. Acad. Sci. USA* **2007**, *104*, 2086.
10. Baird, M. A.; Shliaha, P. V.; Anderson, G. A.; Moskovets, E.; Laiko, V.; Makarov, A. A.; Jensen, O. N.; Shvartsburg, A. A. High-Resolution Differential Ion Mobility Separations/Orbitrap Mass Spectrometry without Buffer Gas Limitations. *Anal. Chem.* **2019**, *91*, 6918.
11. Tao, Y.; Quebbemann, N. R.; Julian, R. R. Discriminating D-Amino Acid-Containing Peptide Epimers by Radical-Directed Dissociation Mass Spectrometry. *Anal. Chem*. **2012**, *84*, 6814.
12. Han, X. *Lipidomics: Comprehensive Mass Spectrometry of Lipids*; Wiley: New York, **2016**.
13. Bowman, A. P.; Abzalimov, R. R.; Shvartsburg, A. A. Broad Separation of Isomeric Lipids by High-Resolution Differential Ion Mobility Spectrometry with Tandem Mass Spectrometry. *J. Am. Soc. Mass Spectrom.* **2017**, *28*, 1552.
14. Singer, D.; Kuhlmann, J.; Muschket, M.; Hoffman, R. Separation of Multiphosphorylated Peptide Isomers by Hydrophilic Interaction Chromatography on an Aminopropyl Phase. *Anal. Chem.* **2010**, *82*, 6409.
15. Berthias, F.; Baird, M. A.; Shvartsburg, A. A. Differential Ion Mobility Separations of D/L Peptide Epimers. *Anal. Chem*. **2021**, *93*, 4015.
16. Mason, E. A.; McDaniel, E. W. *Transport Properties of Ions in Gases*; Wiley: NY, **1988**.
17. Guevremont, R. High-Field Asymmetric Waveform Ion Mobility Spectrometry - a New Tool for Mass Spectrometry. *J. Chromatogr. A* **2004**, *1058*, 3.
18. Shvartsburg, A. A. *Differential Ion Mobility Spectrometry*; CRC Press: Boca Raton, FL, **2008**.
19. Eiceman, G. A., Karpas, Z., Hill, H. H. *Ion Mobility*
20. Shvartsburg, A. A.; Smith, R. D. Scaling of the Resolving Power and Sensitivity for Planar FAIMS and Mobility-Based DIscromination in Flow- and Field- Driven Analyzers. *J. Am. Soc. Mass Spectrom.* **2007**, *18*, 1672.
21. Mesleh, M. F.; Hunter, J. M.; Shvartsburg, A. A.; Schatz, G. C.; Jarrold, M. F. Structural Information from Ion Mobility

Measurements: Effects of the Long-Range Potential. *J. Phys. Chem. A* **1996**, *100*, 16082.

22. Ruotolo, B. T.; Benesch, J. L. P.; Sandercock, A. M.; Hyung, S. J.; Robinson. C. V. Ion Mobility - Mass Spectrometry Analysis of Large Protein Complexes. *Nat. Protocols* **2008**, *3*, 1139.

23. Muccio, Z.; Jackson, G. P. Isotope Ratio Mass Spectrometry. *Analyst* **2009**, *134*, 213.

24. Harsha, H. C.; Molina, H.; Pandey, A. Quantitative Proteomics Using Stable Isotope Labeling with Amino Acids in Cell Culture. *Nat. Protocols* **2008**, *3*, 505.

25. Shi, S. D.; Hendrickson, C. L.; Marshall, A. G. Counting Individual Sulfur Atoms in a Protein by Ultrahigh-Resolution Fourier Transform Ion Cyclotron Resonance Mass Spectrometry: Experimental Resolution of Isotopic Fine Structure in Proteins. *Proc. Natl Acad. Sci. USA* **1998**, *95*, 11532.

26. Nikolaev, E. N.; Jertz, R.; Grigoryev, A.; Baykut, G. Fine Structure in Isotopic Peak Distributions Measured Using a Dynamically Harmonized Fourier Transform Ion Cyclotron Resonance Cell at 7 T. *Anal. Chem*. **2012**, *84*, 2275.

27. Denisov, E.; Damoc, E; Lange, O.; Makarov, A. Orbitrap Mass Spectrometry with Resolving Powers Above 1,000,000. *Int. J. Mass Spectrom.* **2012**, *325 - 327*, 80.

28. Zhurov, K. O.; Kozhinov, A. N.; Tsybin, Y. O. Evaluation of High-Field Orbitrap Fourier Transform Mass Spectrometer for Petroleomics. *Energy Fuels* **2013**, *27*, 2974.

29. Shvartsburg, A. A.; Clemmer, D. E.; Smith, R. D. Isotopic Effect on Ion Mobility and Separation of Isotopomers by High-Field Ion Mobility Spectrometry. *Anal. Chem.* **2010**, *82*, 8047.

30. Wojcik, R.; Nagy, G.; Attah, I. K.; Webb, I. K.; Garimella, S. V. B.; Weitz, K. K.; Hollerbach, A.; Monroe, M. E.; Ligare, M. R.; Nielson, F. F., et al. SLIM Ultrahigh Resolution Ion Mobility Spectrometry Separations of Isotopologues and Isotopomers Reveal Mobility Shifts due to Mass Distribution Changes. *Anal. Chem.* **2019**, *91*, 11952.

31. Harrilal, C. P.; Gandhi, V. D.; Nagy, G.; Chen, X.; Buchanan, M. G.; Wojcik, R.; Conant, C. R.; Donor, M. T.; Ibrahim, Y. M.; Garimella, S. V. B., et al. Measurement and Theory of Gas-Phase Ion Mobility Shifts Resulting from Isotopomer Mass Distribution Changes. *Anal. Chem.* **2021**, *93*, 14966

.32. Kaszycki, J. L.; Baird, M. A.; Shvartsburg, A. A. Molecular Structure Characterization by Isotopic Splitting in Nonlinear Ion Mobility Spectra. *Anal. Chem.* **2018**, *90*, 669.

33. Pathak, P.; Baird, M. A.; Shvartsburg, A. A. Identification of Isomers by Multidimensional Isotopic Shifts in High-Field Ion Mobility Spectra. *Anal. Chem.* **2018**, *90*, 9410.

34. Baird, M. A.; Pathak, P.; Shvartsburg, A. A. Elemental Dependence of Structurally Specific Isotopic Shifts in High-Field Ion Mobility Spectra. *Anal. Chem*. **2019**, *91*, 3687.

35. Pathak, P.; Baird, M. A.; Shvartsburg, A. A. Structurally Informative Isotopic Shifts in Ion Mobility Spectra for Heavier Species. *J. Am. Soc. Mass Spectrom.* **2020**, *31*, 137.

36. Pathak, P.; Sarycheva, A.; Baird, M. A.; Shvartsburg, A. A. Delineation of Isomers by the ^{13}C Shifts in Ion Mobility Spectra. *J. Am. Soc. Mass Spectrom*. **2021**, *32*, 340.

37. Williamson D. L.; Nagy, G. Isomer and Conformer-Specific Mass Distribution-Based Isotopic Shifts in High-Resolution Cyclic Ion Mobility Separations. *Anal. Chem.* **2022**, *94*, 12890.

38. Kaszycki, J. L.; Bowman, A. P.; Shvartsburg, A. A. Ion Mobility Separation of Peptide Isotopomers. *J. Am. Soc. Mass Spectrom*. **2016**, *27*, 795.

39. Williamson, D. L.; Bergman, A. E.; Heider, E. C.; Nagy, G. Experimental Measurements of Relative Mobility Shifts Resulting from Isotopic Substitutions with High-Resolution Cyclic Ion Mobility Separations. *Anal. Chem.* **2022**, *94*, 2988.

40. Shvartsburg, A. A.; Tang, K.; Smith, R. D. Understanding and Designing Field Asymmetric Waveform Ion Mobility Spectrometry Separations in Gas Mixtures. *Anal. Chem.* **2004**, *76*, 7366.

41. Baird, M. A.; Anderson, G. A.; Shliaha, P. V.; Jensen, O. N.; Shvartsburg, A. A. Differential Ion Mobility Separations/Mass Spectrometry with High Resolution in Both Dimensions. *Anal. Chem.* **2018**, *91*, 1479.

42. Staš, M.; Chudoba, J.; Kubička, D.; Pospíšil, M. Chemical Characterization of Pyrolysis Bio-oil: Application of Orbitrap Mass Spectrometry. *Energy Fuels* **2015**, *29*, 3233.

43. Meek, J. M.; Craggs, J. D. *Electrical Breakdown of Gases*; Wiley: NY, **1978**.

44. Shvartsburg, A. A.; Tang, K.; Smith, R. D. FAIMS Operation for Realistic Gas Flow Profile and Asymmetric Waveforms Including Electronic Noise and Ripple. *J. Am. Soc. Mass Spectrom.* **2005**, *16*, 1447.

45. Gorshkov, M. V.; Fornelli, L.; Tsybin, Y. O. Observation of Ion Coalescence in Orbitrap Fourier Transform Mass Spectrometry. *Rapid Commun. Mass Spectrom.* **2012**, *26*, 1711.

46. Barnett, D. A.; Ells, B.; Guevremont, R.; Purves, R. W.; Viehland, L. Evaluation of Carrier Gases for Use in High-Field Asymmetric Waveform Ion Mobility Spectrometry. *J. Am. Soc. Mass Spectrom.* **2000**, *11*, 1125.

47. Shvartsburg, A. A.; Bryskiewicz, T.; Purves, R. W.; Tang, K.; Guevremont, R.; Smith, R. D. Field Asymmetric Waveform Ion Mobility Spectrometry Studies of Proteins: Dipole Alignment in Ion Mobility Spectrometry? *J. Phys. Chem. B* **2006**, *110*, 21966.

48. Barnett, D. A.; Purves, R. W.; Ells, B.; Guevremont, R. Separation of o-, m-, and p- Phthalic Acids by High-Field Asymmetric Waveform Ion Mobility Spectrometry (FAIMS) Using Mixed Carrier Gases. *J. Mass Spectrom.* **2000**, *35*, 976.

49. Felgett, P. B. On the Ultimate Sensitivity and Practical Performance of Radiation Detectors. *J. Opt. Soc. Am.* **1949**, *39*, 970.

50. Valentine, S. J.; Clemmer, D. E. Treatise on the Measurement of Molecular Masses with Ion Mobility Spectrometry. *Anal. Chem.* **2009**, *81*, 5876.

51. von Philipsborn, W.; Muller, R. ^{15}N-NMR Spectroscopy - New Methods and Applications. *Angew. Chem.* **1986**, *25*, 383.

52. Rienstra, C. M.; Hohwy, M.; Hong, M.; Griffin, R. G. 2D and 3D ^{15}N-^{13}C-^{13}C NMR Chemical Shift Correlation Spectroscopy of Solids: Assignment of MAS Spectra of Peptides. *J. Am. Chem. Soc.* **2000**, *122*, 10979.

TOC Graphics